

ADVANCED DEEP NETWORKS FOR 3D MITOCHONDRIA INSTANCE SEGMENTATION

Mingxing Li, Chang Chen, Xiaoyu Liu, Wei Huang, Yueyi Zhang, Zhiwei Xiong

University of Science and Technology of China

ABSTRACT

Mitochondria instance segmentation from electron microscopy (EM) images has seen notable progress since the introduction of deep learning methods. In this paper, we propose two advanced deep networks, named Res-UNet-R and Res-UNet-H, for 3D mitochondria instance segmentation from Rat and Human samples. Specifically, we design a simple yet effective anisotropic convolution block and deploy a multi-scale training strategy, which together boost the segmentation performance. Moreover, we enhance the generalizability of the trained models on the test set by adding a denoising operation as pre-processing. In the Large-scale 3D Mitochondria Instance Segmentation Challenge, our team ranks the 1st on the leaderboard at the end of the testing phase. Code is available at <https://github.com/Limingxing00/MitoEM2021-Challenge>

Index Terms— Electron microscopy, mitochondria, instance segmentation, deep network

1. INTRODUCTION

As an important kind of organelle, mitochondria provide energy for cells and are of great value to the research of life science. Generally, electron microscopy (EM) images that contain recognizable mitochondria consume a huge storage, e.g., at the scale of Terabyte [1]. Manual instance segmentation of mitochondria from such a large amount of data is impossible, and automatic segmentation algorithms are highly desired. As pioneer works, Lucci et al. [2] propose a supervoxel-based method with learned shape features to recognize mitochondria. Seyedhosseini et al. [3] use algebraic curves and a random forest classifier to segment mitochondria. Due to the limited generalizability, however, these traditional methods cannot be easily adapted to large-scale datasets such as MitoEM [4] including both rat and human samples.

Recently, some methods based on convolutional neural networks (CNNs) have emerged for mitochondrial segmentation. For example, Oztel et al. [5] propose a deep network to first segment 2D mitochondria slices and then integrate 3D information with median filtering in the axial dimension. Wei et al. [4] summarize the CNN-based methods into two groups, top-down methods and bottom-up methods. Representative top-down methods use Mask-RCNN [6] for instance segmen-

tion. Due to the elongated and distorted shape of mitochondria, however, it is difficult to set a proper anchor size for Mask-RCNN in this task. The bottom-up methods usually predict a binary segmentation mask [7], an affinity map [8], or a binary mask with the instance boundary [9]. Then a post-processing algorithm is used to distinguish instances. Despite of the notable progress achieved, there is still a large room for improving the performance of mitochondria instance segmentation.

In this paper, we propose two advanced deep residual networks based on the 3D UNet backbone [10], named Res-UNet-R for the rat sample and Res-UNet-H for the human sample in the MitoEM dataset. Both networks generate the same form of outputs, including a semantic mask and an instance boundary. Since the human sample is more difficult (i.e., containing more noise) than the rat sample, we increase a decoder path for Res-UNet-H to predict the semantic mask and the instance boundary separately, while the decoder of Res-UNet-R has only one path. Obtaining the semantic mask and the instance boundary, we then synthesize a seed map. Finally, we adopt the connected component labeling to obtain the mitochondria instances.

To boost the segmentation performance of our networks, we design a simple yet effective anisotropic convolution block and deploy a multi-scale training strategy. The effectiveness of these two components is validated by comprehensive experiments. Moreover, we observe that noise caused by staining precipitates is sparsely distributed in the MitoEM dataset. Especially in the human sample, the noise level is subjectively stronger than that in the rat sample. To alleviate the influence of noise on segmentation, we utilize an interpolation network [11, 12] to restore the noisy regions coarsely marked by labor. It is demonstrated that the generalizability of the trained models can be enhanced on the test set by adding this denoising operation as pre-processing.

2. METHOD

2.1. Res-UNet-R and Res-UNet-H

We follow the bottom-up methods to extract the response map of mitochondria first. For the rat sample and the human sample, we propose two deep residual networks named Res-UNet-R and Res-UNet-H respectively. In the following description, we omit the exponential linear unit (ELU) after

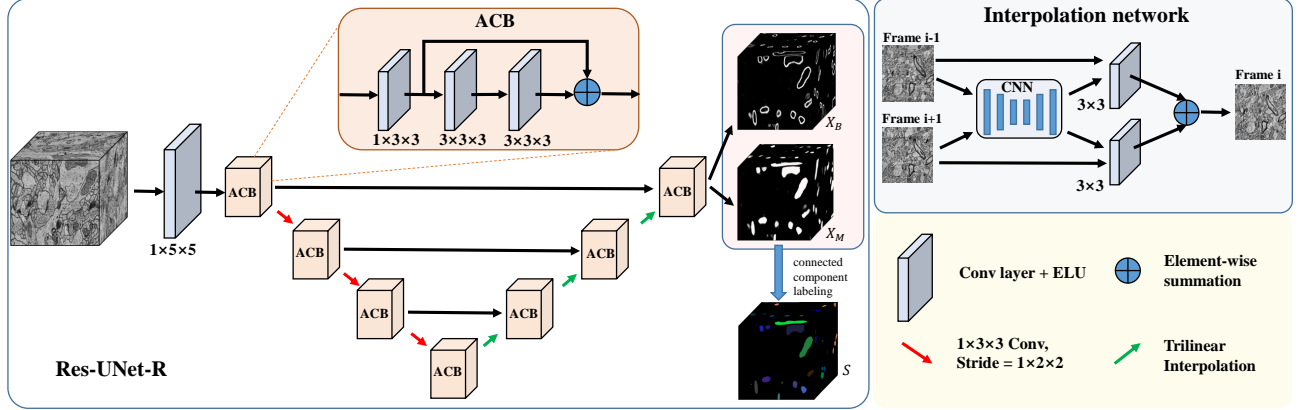


Fig. 1. Network structure of Res-UNet-R. Note that the decoder of Res-UNet-H has two paths to generate the semantic mask and the instance boundary separately.

the convolutional layer for brevity.

Anisotropic Convolution Block. Since the MitoEM dataset has anisotropic resolution, we design an anisotropic convolution block (ACB) as shown in Fig. 1. After a $1 \times 3 \times 3$ conventional layer, we cascade two $3 \times 3 \times 3$ conventional layers to further enlarge the receptive field. At the same time, we insert the skip connection in the two $3 \times 3 \times 3$ conventional layers.

Network Structure. The overall structure of Res-UNet-R is shown in Fig. 1. Inspired by 3D U-Net [10], we first embed the feature maps extracted from a 3D block with a $1 \times 5 \times 5$ convolutional layer. In each layer of the encoder, there is an ACB to extract the anisotropic information. Then we adopt a $1 \times 3 \times 3$ convolutional layer to downsample the feature maps in the lateral dimensions. In the decoder, we use the trilinear upsampling to restore the resolution of the feature maps and the ACB to reconstruct the detailed information. For Res-UNet-R, the decoder outputs a semantic mask and an instance boundary simultaneously. Since the human sample is of poorer imaging quality than the rat sample, we design two decoder paths for Res-UNet-H to predict the semantic mask and the instance boundary separately.

Loss Function. The binary cross entropy (BCE) is a common loss function used in biomedical image segmentation. To address the class imbalance problem, we adopt a weighted BCE (WBCE) loss as

$$L_{WBCE}(\mathbf{X}_i, \mathbf{Y}_i) = \frac{1}{DHW} \mathbf{W}_i L_{BCE}(\mathbf{X}_i, \mathbf{Y}_i), \quad (1)$$

where \mathbf{X}_i and \mathbf{Y}_i are the predicted response map and ground-truth of the i -th block, D , H , and W denote the depth, height, and width of the block, and the weight \mathbf{W}_i is defined as

$$\mathbf{W}_i = \begin{cases} \mathbf{Y}_i + \frac{W_f}{1-W_f}(1 - \mathbf{Y}_i) & W_f > 0.5 \\ \frac{1-W_f}{W_f} \mathbf{Y}_i + (1 - \mathbf{Y}_i) & else \end{cases} \quad (2)$$

Here W_f is the foreground voxel ratio, i.e., $W_f = \frac{\text{sum}(\mathbf{Y}_i)}{DHW}$.

The overall loss function L is defined as

$$L = L_{WBCE}(\mathbf{X}_M, \mathbf{Y}_M) + L_{WBCE}(\mathbf{X}_B, \mathbf{Y}_B), \quad (3)$$

where \mathbf{X}_M and \mathbf{X}_B are the predicted response maps of the semantic mask and the instance boundary respectively. \mathbf{Y}_M and \mathbf{Y}_B are the corresponding ground-truth of \mathbf{X}_M and \mathbf{X}_B .

2.2. Post-processing

Obtaining the semantic mask $\mathbf{X}_M \in \mathbb{R}^{D \times H \times W}$ and the instance boundary $\mathbf{X}_B \in \mathbb{R}^{D \times H \times W}$, we can generate the seed map $\mathbf{S}^j (j \in [1, D \times H \times W])$ as

$$\mathbf{S}^j = \begin{cases} 1 & \mathbf{X}_M^j > T_1, \mathbf{X}_B^j < T_2 \\ 0 & else \end{cases} \quad (4)$$

where T_1 and T_2 are two thresholds. In our experiments, we set $T_1 = 0.9$ and $T_2 = 0.8$. Then we generate the seed map and adopt the connected component labeling to obtain the final mitochondria instances.

2.3. Denoising as Pre-processing

As mentioned above, we find that by adding a denoising operation as pre-processing on the test set, the influence of noisy regions on segmentation can be alleviated, especially for the human sample. To this end, we adopt the interpolation network initially proposed for video frame [11] and also employed for EM image restoration in [12]. As shown in Fig. 1, the interpolation network takes the two adjacent frames of the noisy frame as input and predicts two kernels. The two adjacent frames are then convolved by the two kernels respectively, the sum of which contributes to the restored frame. Fig. 2 gives visual examples of frames before and after denoising, which demonstrate the effectiveness of the denoising pre-processing.

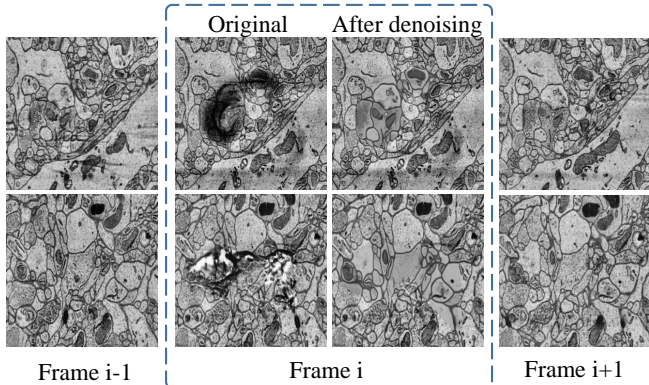


Fig. 2. Visualized results before and after denoising pre-processing on the test set of MitoEM-H.

3. EXPERIMENTS

3.1. Dataset and Evaluation Metric

The MitoEM dataset [4] consists of two $(30 \mu m)^3$ EM image volumes of resolution $8 \times 8 \times 30 nm$, which come from a rat tissue (MitoEM-R) and a human tissue (MitoEM-H) respectively. The two volumes have been stitched and aligned. Each volume has three parts, a training set ($400 \times 4096 \times 4096$), a validation set ($100 \times 4096 \times 4096$) and a test set ($500 \times 4096 \times 4096$).

We adopt an efficient 3D metric, which evaluates AP-75 with the bounding boxes instead of voxel-wise calculation [4]. In this case, at least 0.75 intersection over union (IoU) with the ground truth for a detection is required to be a true positive (TP). According to the number of mitochondrial voxels, mitochondria are divided into small, medium and large instances, with respective thresholds of 5K and 15K.

3.2. Implementation Details

We adopt Pytorch (version 1.1) to implement the proposed method. Two TITAN Xp (12GB) are used for training and inference. During the training stage, we adopt the 11 data augmentation methods following [4] and set the batch size as 2. The network is optimized by Adam with a fixed learning rate 0.0001. We train the network in two stages. First, we train the network in 20K iterations with the input size $32 \times 256 \times 256$ to select the best model. Then we change the input size to $36 \times 320 \times 320$ and fine-tune the network in 10K iterations. We call this two-stage training as multi-scale training. The validation stage needs 45 GB of memory, which is mainly due to post-processing for the seed map of size $3 \times 100 \times 4096 \times 4096$.

We train the interpolation network with $3 \times 256 \times 256$ patches in the training set. The interpolation network is responsible for predicting the middle slice of the patch supervised by the mean square error (MSE) loss. We manu-

Block unit	MitoEM-R			
	Small	Med	Large	ALL
3D ECA block	0.398	0.831	0.874	0.865
3D SE block	0.388	0.826	0.891	0.872
3D Res block	0.375	0.860	0.901	0.884
3D ACB	0.307	0.853	0.935	0.913
3D ACB+MT	0.277	0.850	0.949	0.917

Table 1. Segmentation results on MitoEM-R validation set.

Method	MitoEM-H			
	Small	Med	Large	ALL
Res-UNet-R	0.470	0.791	0.790	0.783
Res-UNet-H	0.405	0.805	0.837	0.816
Res-UNet-H+MT	0.522	0.844	0.826	0.828

Table 2. Segmentation results on MitoEM-H validation set.

Method	MitoEM-R			
	Small	Med	Large	ALL
Res-UNet-R	0.305	0.861	0.848	0.850
After denoising	0.151	0.832	0.854	0.851
Method	MitoEM-H			
	Small	Med	Large	ALL
Res-UNet-H	0.522	0.844	0.826	0.828
After denoising	0.531	0.834	0.827	0.829

Table 3. Segmentation results on test sets of MitoEM-R and MitoEM-H .

ally mark the coarse noisy regions on the test sets of both MitoEM-R and MitoEM-H and utilize the trained interpolation network to restore the noisy regions before inference of segmentation.

3.3. Ablation Study

We conduct comprehensive experiments to validate the effectiveness of main components in the proposed method.

Block Unit Selection. We test different block units in Table 1 on the validation set of MitoEM-R. Here 3D SE block [13], 3D ECA block [14] and 3D Res block [15] are modified from state-of-the-art methods for the image recognition task. In comparison with these more complex block units, our simply designed ACB alleviates overfitting and achieves the best results on the 3D mitochondria segmentation task, outperforming the second best method by 2.9%.

Network Structure. As shown in Table 2, if we train and test Res-UNet-R on MitoEM-H, the AP-75 result is 0.783. By introducing an extra decoder, Res-UNet-H improves the AP-75 result to 0.816 (3.3% increment). It verifies that Res-UNet-H can handle more difficult sample.

Training Strategy. As shown in Table 1 and 2, the multi-scale training strategy (MT) we used is beneficial for both

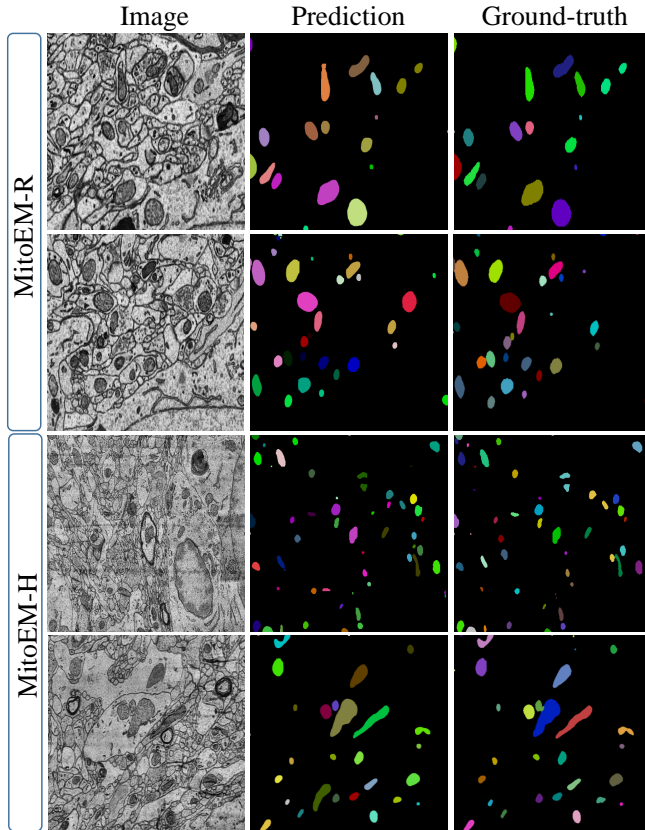


Fig. 3. Visualized results from validation sets of MitoEM-R and MitoEM-H.

models, especially for Res-UNet-H (AP-75 improves 1.2%). It proves that both models need larger receptive field to avoid over-fitting.

Denoising Pre-processing. As shown in Fig. 2, the noisy regions of the middle frame can be well restored by the interpolation network. We evaluate the effect of denoising pre-processing with the above trained segmentation models on the test sets of both MitoEM-R and MitoEM-H. As shown in Table 3, the AP-75 metric improves 0.1% on both test sets.

3.4. Challenge Results

In the Large-scale 3D Mitochondria Instance Segmentation Challenge, our team ranks the 1st on the leaderboard at the end of the testing phase. As shown in Table 4, the proposed method notably outperforms other competitors on both MitoEM-R and MitoEM-H test sets. We also show some visualized results from the validation set of MitoEM-R and MitoEM-H in Fig.3. It can be seen that the predicted results by the proposed method is very close to ground-truth.

4. CONCLUSION

In this paper, we present two advanced deep networks for 3D mitochondria instance segmentation, named Res-UNet-

Method	MitoEM-R	MitoEM-H	Average
Ours	0.851	0.829	0.8400
2nd	0.836	0.800	0.8180
3rd	0.833	0.800	0.8165
4th	0.816	0.804	0.8100

Table 4. MitoEM Challenge leaderboard at the end of the testing phase.

R for the rat sample and Res-UNet-H for the human sample. Specifically, we exploit a simple yet effective ACB and a multi-scale training strategy to boost the segmentation performance. Moreover, we enhance the generalizability of the trained models on the test set by adding a denoising operation as pre-processing. In the Large-scale 3D Mitochondria Instance Segmentation Challenge, our team ranks the 1st on the leaderboard at the end of the testing phase.

5. REFERENCES

- [1] Alessandro Motta et al., “Dense connectomic reconstruction in layer 4 of the somatosensory cortex,” *Science*, vol. 366, no. 6469, 2019.
- [2] Aurélien Lucchi et al., “Supervoxel-based segmentation of mitochondria in em image stacks with learned shape features,” *IEEE transactions on medical imaging*, vol. 31, no. 2, pp. 474–486, 2011.
- [3] Mojtaba Seyedhosseini, Mark H Ellisman, and Tolga Tasdizen, “Segmentation of mitochondria in electron microscopy images using algebraic curves,” in *ISBI*, 2013.
- [4] Donglai Wei, Zudi Lin, et al., “Mitoem dataset: Large-scale 3d mitochondria instance segmentation from em images,” in *MICCAI*, 2020.
- [5] Ismail Oztel, Gozde Yolcu, Ilker Ersoy, Tommi White, and Filiz Buncak, “Mitochondria segmentation in electron microscopy volumes using deep convolutional neural network,” in *BIBM*, 2017.
- [6] Kaiming He, Georgia Gkioxari, Piotr Dollár, and Ross Girshick, “Mask r-cnn,” in *ICCV*, 2017.
- [7] Olaf Ronneberger, Philipp Fischer, and Thomas Brox, “U-net: Convolutional networks for biomedical image segmentation,” in *MICCAI*, 2015.
- [8] Kisuk Lee, Jonathan Zung, Peter Li, Viren Jain, and H Sebastian Seung, “Superhuman accuracy on the snemi3d connectomics challenge,” *arXiv preprint arXiv:1706.00120*, 2017.
- [9] Hao Chen, Xiaojuan Qi, Lequan Yu, and Pheng-Ann Heng, “Dcan: deep contour-aware networks for accurate gland segmentation,” in *CVPR*, 2016.
- [10] Özgün Çiçek et al., “3d u-net: learning dense volumetric segmentation from sparse annotation,” in *MICCAI*, 2016.
- [11] Simon Niklaus, Long Mai, and Feng Liu, “Video frame interpolation via adaptive convolution,” in *CVPR*, 2017.
- [12] Wei Huang, Chang Chen, Zhiwei Xiong, Yueyi Zhang, Dong Liu, and Feng Wu, “Learning to restore sstem images from deformation and corruption,” in *ECCV*, 2020.
- [13] Jie Hu, Li Shen, and Gang Sun, “Squeeze-and-excitation networks,” in *CVPR*, 2018.
- [14] Qilong Wang et al., “Eca-net: Efficient channel attention for deep convolutional neural networks,” in *CVPR*, 2020.
- [15] Kaiming He, Xiangyu Zhang, Shaoqing Ren, and Jian Sun, “Deep residual learning for image recognition,” in *CVPR*, 2016.